

Supplementary Information

An oxygen-blocking oriented multifunctional solid-electrolyte interphase as a protective layer for a lithium metal anode in lithium–oxygen batteries

Xiao-Dong Lin,[‡]^a Yu Gu,[‡]^a Xiao-Ru Shen,^a Wei-Wei Wang,^a Yu-Hao Hong,^a Qi-Hui Wu,^b Zhi-You Zhou,^a De-Yin Wu,^a Jeng-Kuei Chang,^c Ming-Sen Zheng,^{*a} Bing-Wei Mao^{*a} and Quan-Feng Dong^{*a}

^aCollaborative Innovation Center of Chemistry for Energy Materials (*i*ChEM), State Key Laboratory of Physical Chemistry of Solid Surfaces, Department of Chemistry, College of Chemistry and Chemical Engineering, Engineering Research Center of Electrochemical Technologies of Ministry of Education, Xiamen University, Xiamen 361005, China

^bCollege of Mechanical and Energy Engineering, Jimei University, Xiamen 361021, China

^cDepartment of Materials Science and Engineering, National Chiao Tung University, Hsinchu 30010, Taiwan

[‡]These authors contributed equally to this work.

*Correspondence: qfdong@xmu.edu.cn; bwmao@xmu.edu.cn; mszheng@xmu.edu.cn

Supplementary Experimental Section

Chemicals and Materials

Sodium nitrate (NaNO₃, AR), potassium permanganate (KMnO₄, AR), sulfuric acid (H₂SO₄, AR, 98 wt.%), and hydrogen peroxide (H₂O₂, AR, 30 wt.%) were purchased from Sinopharm. RuCl₃·xH₂O was purchased from Alfa Aesar. Expanded graphite was purchased from Qingdao Tianheda Graphite Co., Ltd. Carbon cloth (CC) was purchased from Shanghai Heseng electric Co., Ltd. The lithium (Li) metal foils (Φ16 × 1.0 mm, ≥99.9%) used in this work were purchased from Shunyou Metal Co., Ltd. (Shanghai, China). 1 M lithium perchlorate (LiClO₄) in dimethyl sulfoxide (DMSO, H₂O < 20 ppm), DMSO (H₂O < 20 ppm), and 1,2-Dimethoxyethane (DME, H₂O < 20 ppm) were purchased from Fosai New Materials Co., Ltd (Suzhou, China).

Synthesis of Ru/rGO composite

The graphene oxide (GO) was synthesized through a modified Hummers' method. Typically, 0.5 g expanded graphite, 0.5 g NaNO₃, and 3 g KMnO₄ were dispersed uniformly in 60 mL concentrated H₂SO₄ (98 wt.%) under stirring at room temperature for 12 h. The obtained mixture was then slowly poured into ~500 mL deionized (DI) water with continuous stirring. After the suspension cooled down to room temperature, H₂O₂ solution (30 wt.%) was added dropwise to the above suspension until the colour of the suspension turned orange. Later, the orange suspension was centrifuged and washed with DI water for several times to obtain the GO gel. Further, after the thermal reduction of GO that includes a preliminary hydrothermal treatment and a subsequent calcination at 1500 °C under N₂ atmosphere for 3 h, the reduced graphene oxide (rGO) was obtained. To prepare the Ru/rGO composite, 0.2 g rGO and 0.1 g RuCl₃·xH₂O were dispersed in 50 mL DI water under stirring for 2 h to obtain a homogeneous mixture. Subsequently, the resulting suspension was freeze-dried and reduced in a 10 % H₂/Ar mixed atmosphere at 300 °C for 3 h to obtain the final product (Ru/rGO composite).

X-ray diffraction (XRD) measurements

The Li–O₂ batteries were disassembled in glovebox and the discharged and charged electrodes were washed with anhydrous DME several times and dried under vacuum. Then, the dried electrodes were placed in a home-made fluted glass and sealed with a kapton polyimide film before exposed to air. Further, the products of discharged and charged electrodes were detected using X-ray diffraction (XRD), recorded on a Rigaku Ultima IV X-ray diffractometer based on Cu K α radiation ($\lambda = 1.5418 \text{ \AA}$) with a scan angle range of 10–60° for cathode and 19–70° for anode.

Scanning electron microscopy (SEM) measurements

The discharged and charged electrodes used for scanning electron microscopy (SEM) measurements were treated similarly to that of X-ray diffraction measurements. The dried electrodes were immobilized on a SEM sample stage and enclosed into a sealed bag before exposed to air, the sample stage was transferred to the sample chamber and pumped immediately after being taken out from the sealed bag. Then, the nanostructures and surface morphologies of the discharged and charged electrodes were investigated using field emission scanning electron microscopy (FESEM, HITACHI S-4800).

X-ray photoelectron spectroscopy (XPS) measurements

The discharged and charged electrodes used for X-ray photoelectron spectroscopy (XPS) measurements were treated similarly to that of X-ray diffraction measurements. The dried electrodes were immobilized on a XPS sample stage and placed in a gas-tight transfer device, which ensures that the sample stage could be successfully transferred to the sample chamber without exposing to air. Then, the XPS measurements were performed on PHI 5000 Versa Probe II (ULVAC PHI) using monochromatic Al K (1486.6 eV) X ray source at 24 W and 16 KV with a beam spot size of 100 μm . The binding energies were referenced to the C 1s line at 284.6 eV from adventitious carbon. Depth profiling was fulfilled using Ar ion sputtering in the x y scan mode at ion acceleration of 2 kV and ion beam current of 2 μA over an area of 2 \times 2 mm².

The detailed calculation procedure for DEMS data

1. After the DEMS experiment, we introduced a standard gas containing 100ppm O₂ and CO₂ (helium (He) as the balance gas), and then detected the response signal intensity.
2. Taking O₂ signal as an example, after obtaining the original data of the spectrum, we will subtract the baseline first, and then we can obtain the signal intensity S_a of the O₂ with standard P_a=100ppm. Thus, the concentration factor A can be calculated at this time.

$$A = \frac{P_a}{S_a}$$

3. Based on the concentration factor A, the real-time concentration change curve of O₂ during the discharge/charge process of the Li–O₂ battery can be obtained.

$$n_s = \frac{A \cdot S_s \cdot v \cdot p}{R \cdot T}$$

n_s: The amount of O₂ product released per unit time;

A: Concentration factor;

S_s: The mass spectrum response signal intensity of O₂;

v: Calibrated flow rate;

p: The gas pressure (1 atm);

R: Gas constant;

T: Ambient temperature (298 K).

By combining the flow rate parameter and performing the above calculations, a graph of the amount of O₂ consumed per unit time (nmol s⁻¹) during discharge or released per unit time (nmol s⁻¹) during charge can be obtained. Similarly, a corresponding CO₂ curve can also be obtained.

4. For the theoretical 2e⁻/O₂ line, based on the equation of Q=It=nzF, the theoretical amount of O₂ consumed per unit time during discharge or released per unit time during charge can be obtained (n_t=n/t=l/zF). The discharge and charge current we use here are 0.4 mA and 0.1 mA, respectively, and the theoretical electron transfer number (z) is 2 based on the formation or decomposition of Li₂O₂ (Li⁺ + 2e⁻ + O₂ ↔ Li₂O₂). Therefore, the theoretical amount of O₂ consumed per unit time during discharge is about 2.072 nmol s⁻¹ (n_{t,d}=n/t=l/zF=0.4/(2×96500) mmol s⁻¹≈2.072 nmol s⁻¹) while the theoretical amount of O₂ released per unit time during charge is about 0.518 nmol s⁻¹ (n_{t,c}=n/t=l/zF=0.1/(2×96500) mmol s⁻¹≈0.518 nmol s⁻¹).

Considerations on the mutual constrains between electropolishing and SEI formation

The electrochemical polishing of Li metal surface, involving anodic dissolution as the first step (stripping step), distinct with the concurrent reduction of electrolyte and formation of insoluble N-SEI film which is indispensable for protecting Li anode after the polishing. Such approach strongly depends on the exact anodic potential regulation in the stripping step. As judged by CVs (Figure S1), the reduction of electrolyte falls into two potential intervals of higher potential region (0.1~1.5 V) and lower potential region (<0.1 V). Polishing Li surface at any one of these intervals can enable high-rate of Li dissolution, which creates extremely high Li ion concentration to form a viscous Li-rich liquid layer and favors the formation of primary SEI. However, depending on the potential intervals, the reduction sequence of LiNO₃ could vary considerably so that chemical composition of the N-SEI can be manipulated. At a moderate potential (e.g.1.0 V), LiNO₃ can proceed the reduction to high oxidation state (e.g. soluble LiNO₂). Lowering the stripping potential to lower potential region (e.g. <0.1 V) provides stronger driving force for the reduction of LiNO₃, leading to the fast accumulation of the insoluble products of LiNO₃ (e.g. Li₂N₂O₂). In addition, in the plating step, Li deposition is enabled, which anneals the surface by Li back deposition at defect sites. Meanwhile the even more cathodic potential provides strong driving force for LiNO₃ to reduction, which leads to completion of N-SEI with soluble inner layer encapsulated by the insoluble outer layer.

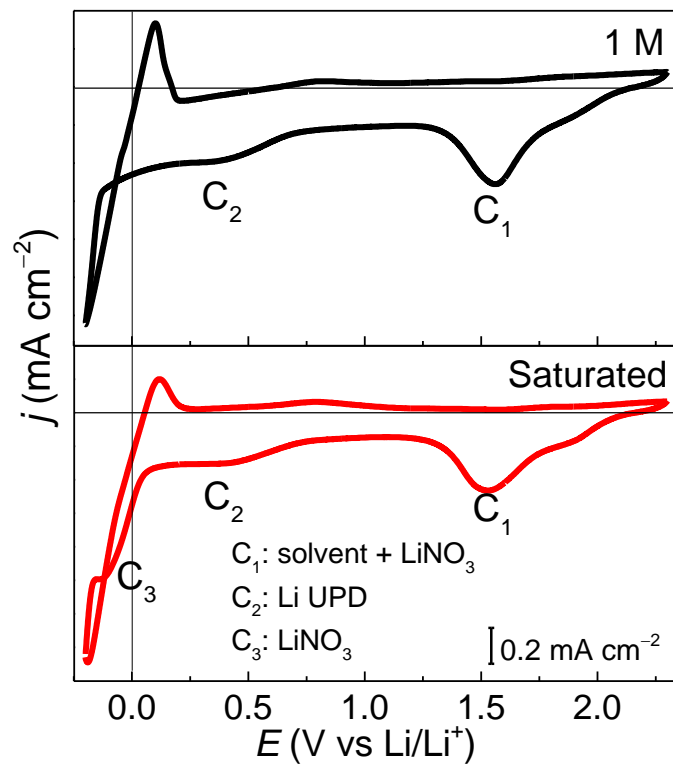


Figure S1. Cyclic voltammograms of a Cu disk electrode in DME-DOL (1:1 by volume) containing 1 M and saturated LiNO_3 , respectively. Scan rate: 50 mV s^{-1} .

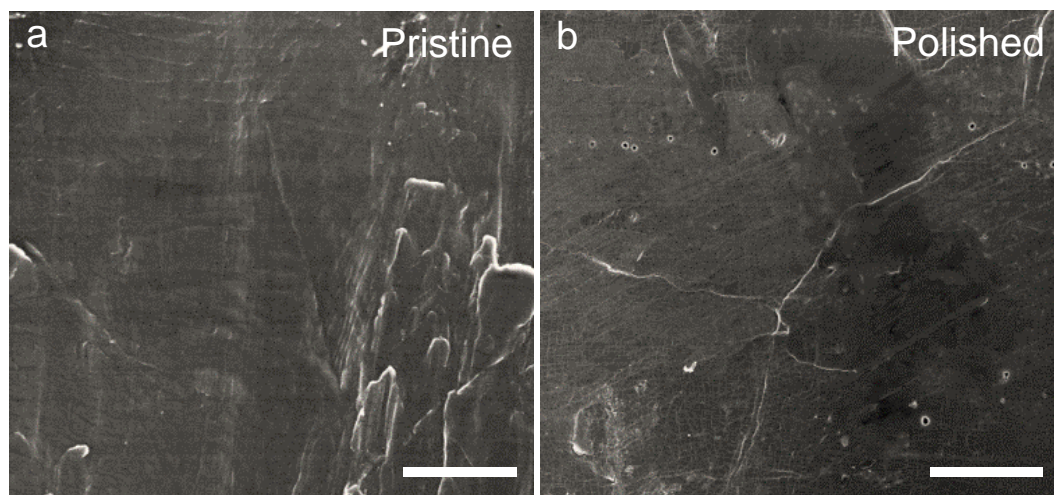


Figure S2. SEM images of pristine (a) and polished (b) Li surfaces, respectively. Scale bar: $50 \mu\text{m}$.

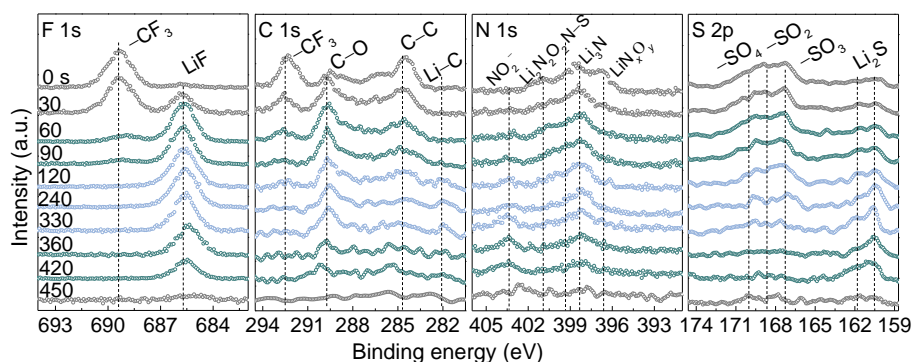


Figure S3. F 1s, C 1s, N 1s, and S 2p XPS depth profiles of the N-SEI film. The thickness of the SEI was estimated to be ~28 nm based on the calibrated sputtering rate of 4 nm per minute for Si.

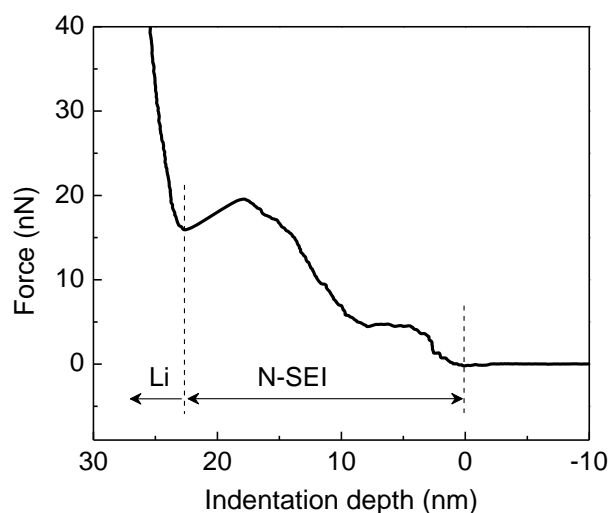


Figure S4. AFM nanoindentation characterization of the N-SEI film.

The successive plateau and sawtooth features are clearly observed on the corresponding force-indentation curve of polished Li electrode covered with N-SEI, which indicates that such SEI possesses a multi-layered structure. The thickness of N-SEI, ca. 23 nm, can also be estimated by counting the length between the onset of force increase up to the point at which the slope of force-indentation curve has a distinct change, which is consistent with the thickness estimated by XPS (ca. 28 nm).

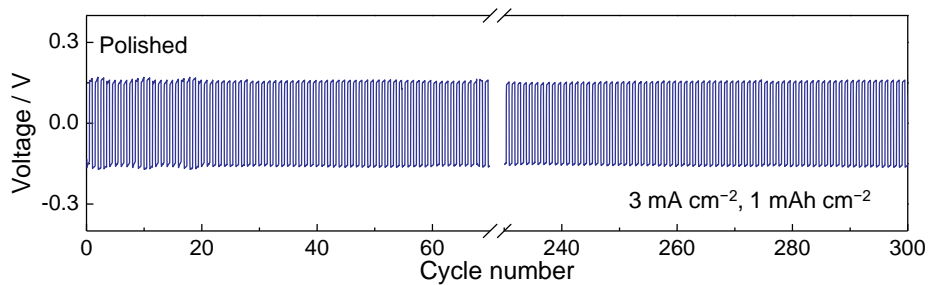


Figure S5. Cycling stability of the symmetric Li cells with polished Li anode in O₂-saturated DMSO electrolyte at 3 mA cm⁻² with a cutoff capacity of 1 mA h cm⁻².

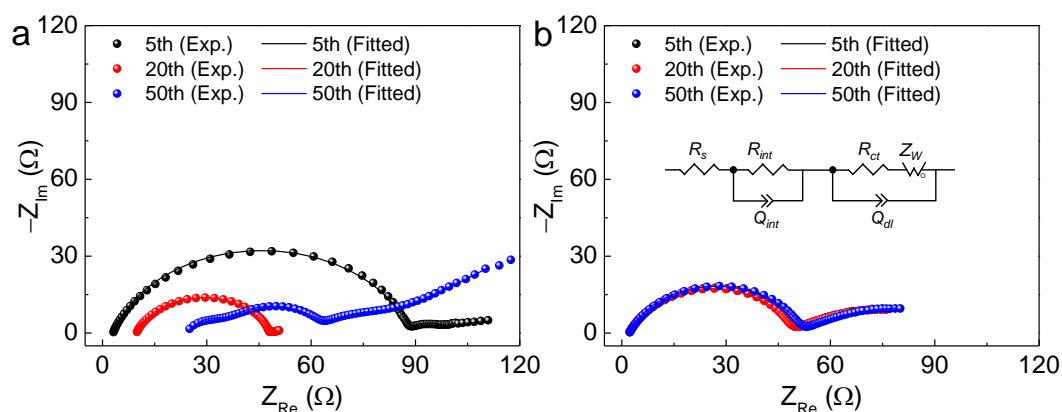


Figure S6. EIS measurements of symmetric Li cells with pristine (a) and LiNO₃-polished (b) Li electrodes taken after different cycles, respectively.

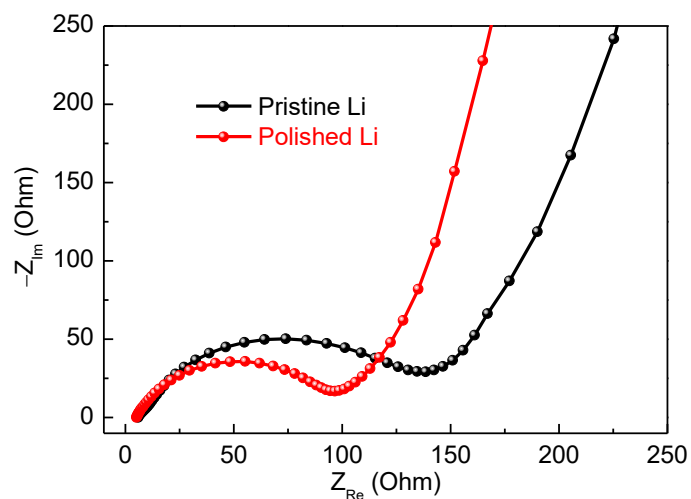


Figure S7. EIS measurements of the Li-O₂ batteries with pristine and polished Li anodes taken after 5 cycles.

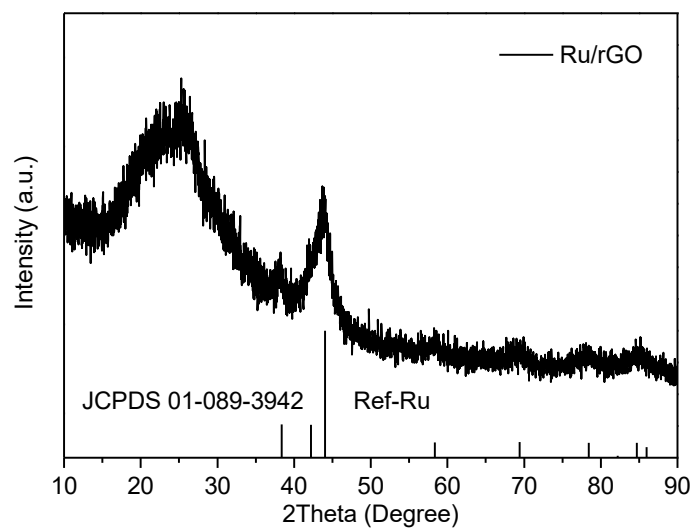


Figure S8. XRD pattern of the Ru/rGO material.

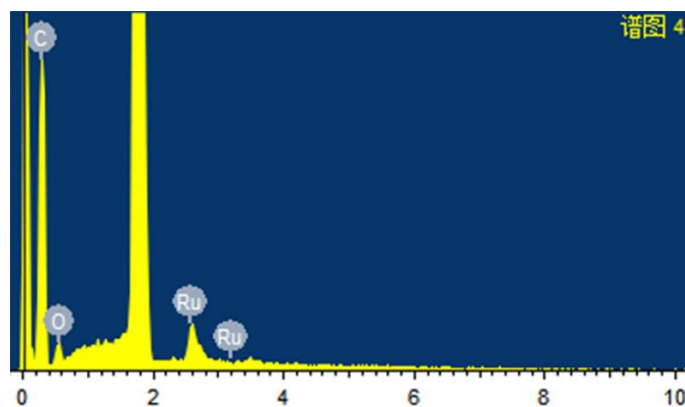


Figure S9. EDS analysis of the Ru/rGO material.

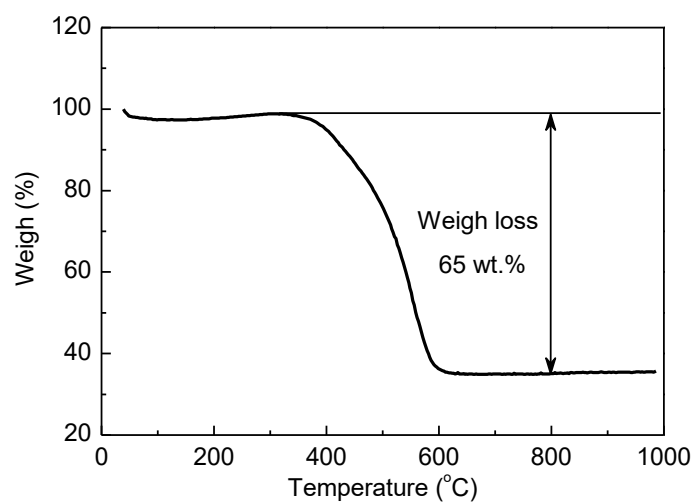


Figure S10. TG curve of the Ru/rGO material. The total weight loss of the sample is about 65 wt.% at 800 °C. Since the Ru nanoparticles would be oxidized to RuO₂ after test, the Ru content in the Ru/rGO composite was calculated to be 26.6 wt.%.

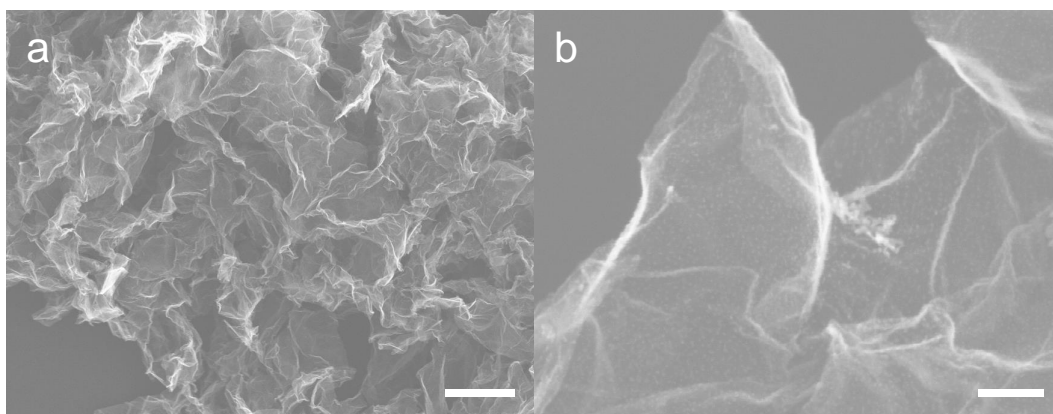


Figure S11. SEM images of the Ru/rGO material with different magnifications. Scare bar: (a) 2 μm ; (b) 0.1 μm .

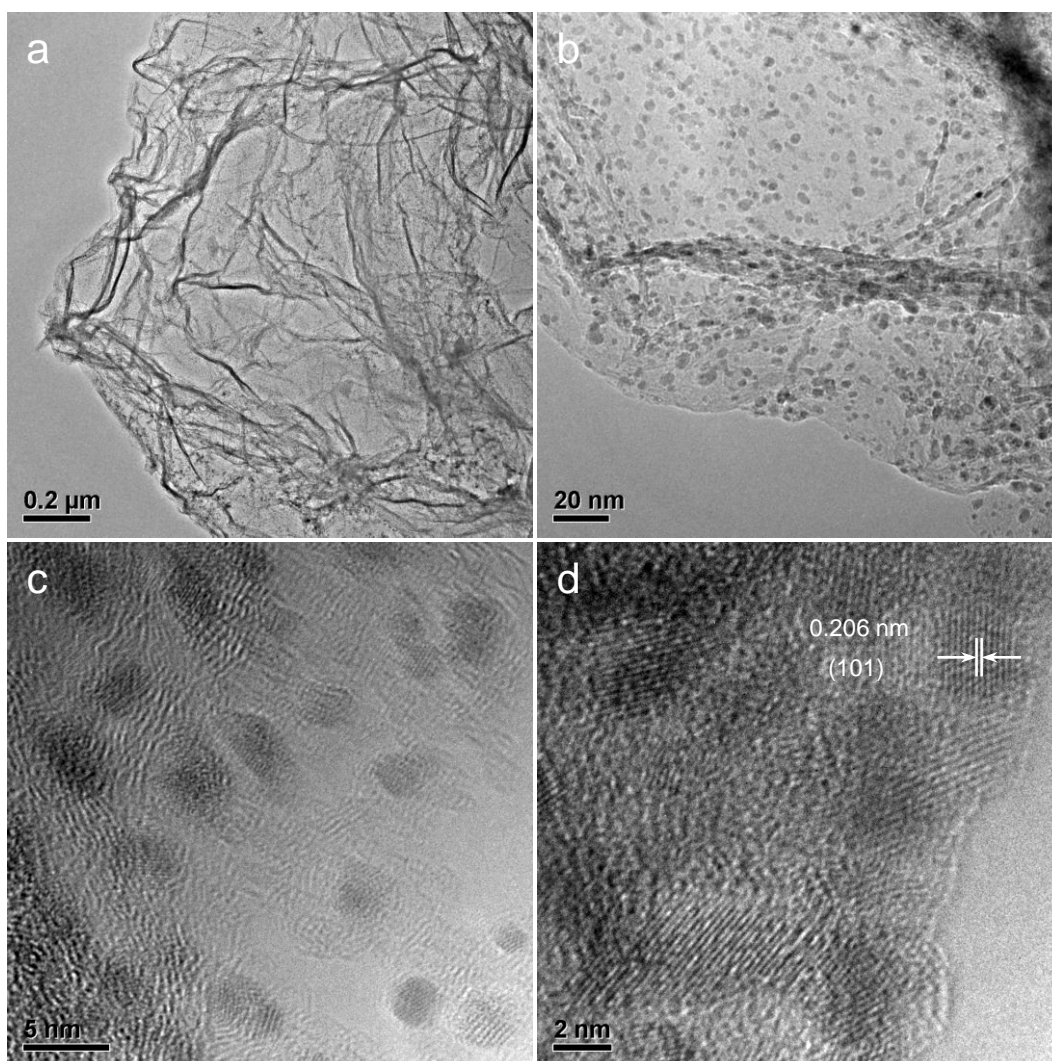


Figure S12. TEM images of the Ru/rGO material with different magnifications.

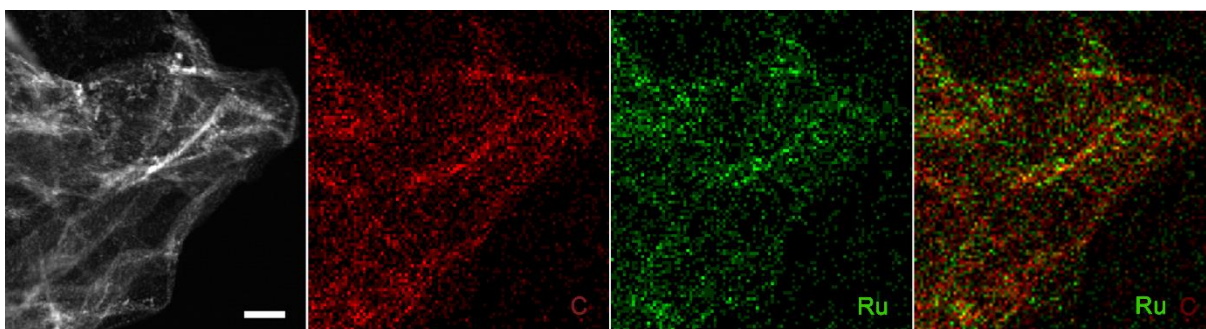


Figure S13. High angle annular dark field-scanning transmission electron microscope (HAADF-STEM) image and corresponding EDX maps of the Ru/rGO material, scale bar: 100 nm.

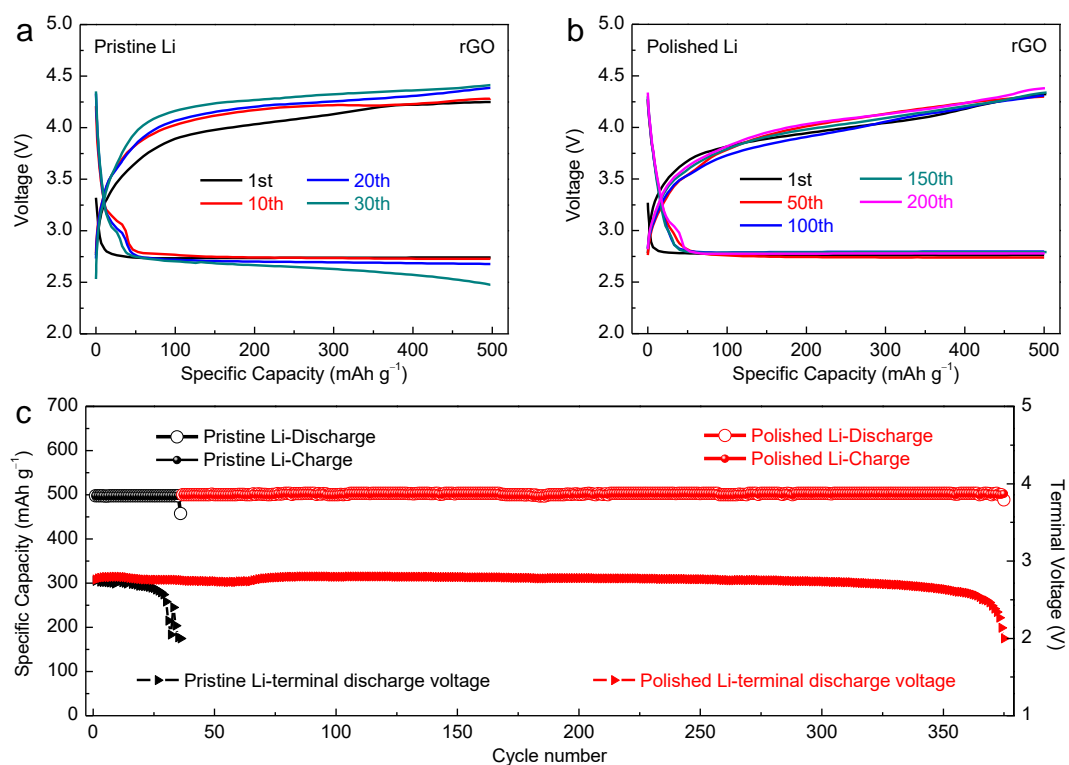


Figure S14. Selected discharge/charge curves of the rGO-based Li-O₂ batteries with pristine (a) and polished (b) under a cutoff capacity of 500 mA h g⁻¹ at a current density of 400 mA g⁻¹, respectively. (c) Cycling stability and the terminal discharge voltage of the rGO-based Li-O₂ batteries with pristine and polished Li anodes under a cutoff capacity of 500 mA h g⁻¹ at a current density of 400 mA g⁻¹.

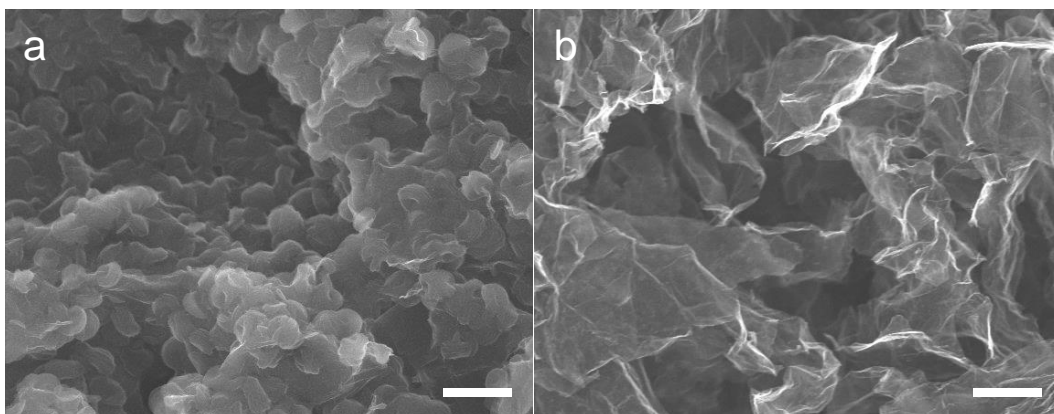


Figure S15. SEM images of the Ru/rGO cathode after discharge (a) and charge (b), respectively. Scale bar: (a) 1 μm; (b) 1 μm.

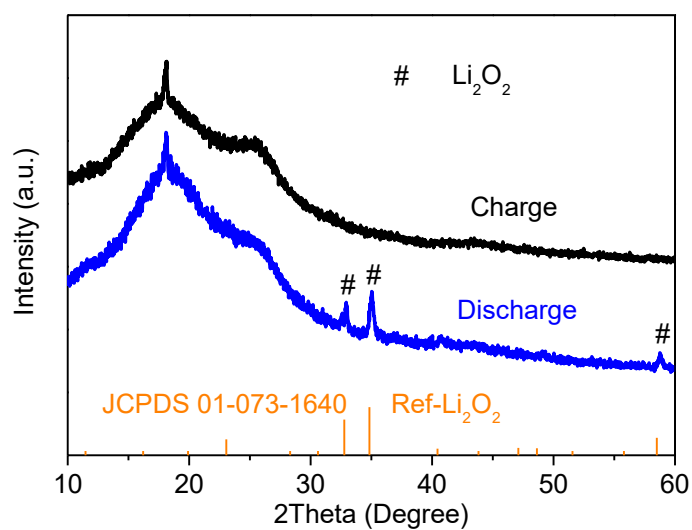


Figure S16. XRD pattern of the Ru/rGO cathode after discharge and charge.

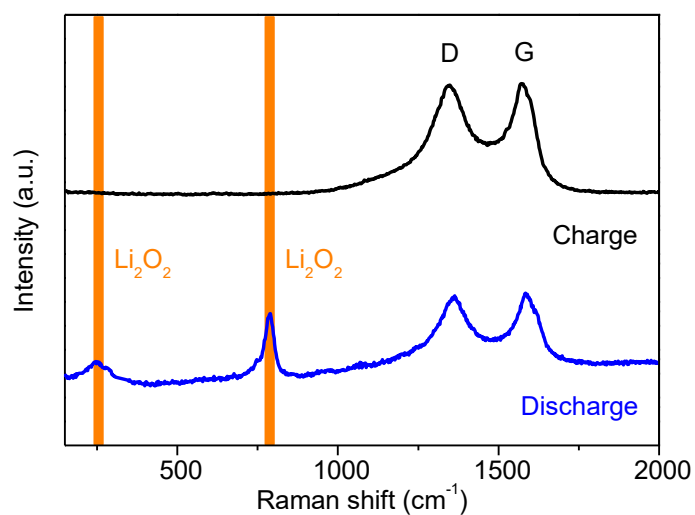


Figure S17. Raman spectra of the Ru/rGO cathode after discharge and charge.

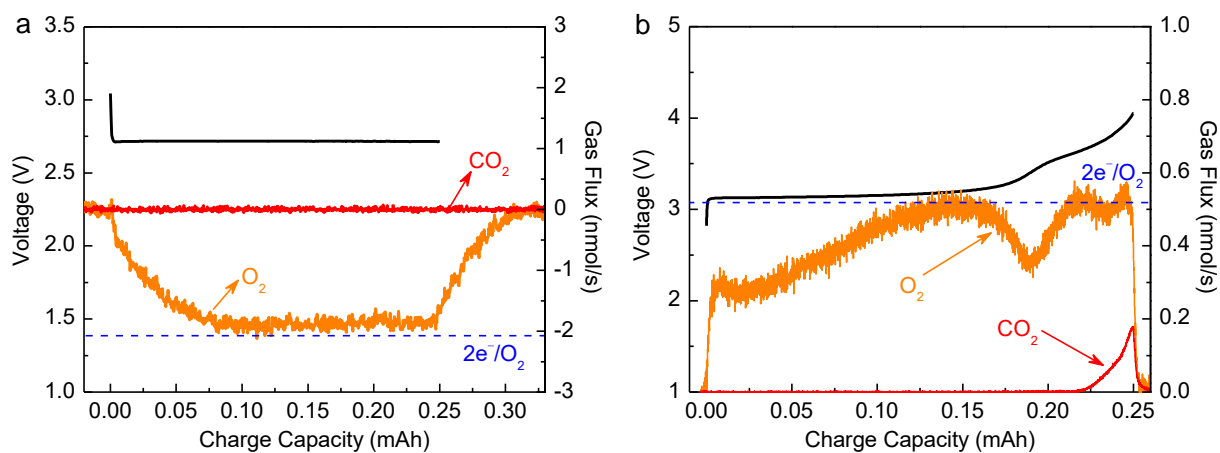


Figure S18. (a) Galvanostatic discharge (at a current of 0.4 mA) profile and corresponding gas consumption rates of the Ru/rGO-based Li–O₂ battery with polished Li anode. (b) Galvanostatic charge (at a current of 0.1 mA) profile and corresponding gas evolution rates of the Ru/rGO-based Li–O₂ battery with polished Li anode.

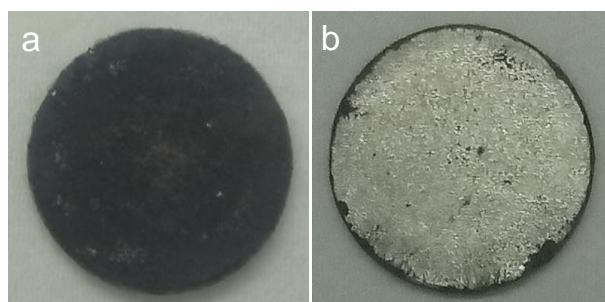


Figure S19. Optical photograph of the pristine (a) and polished (b) Li anodes after cycling for 20 cycles, respectively.

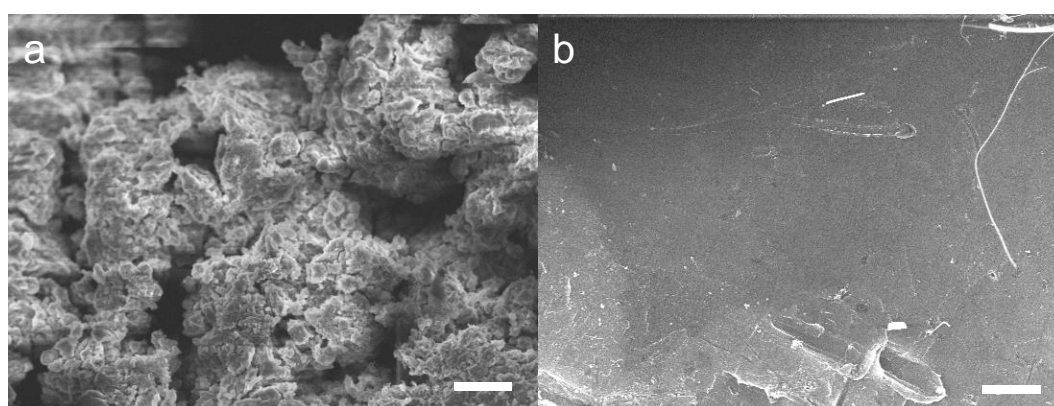


Figure S20. SEM images of the pristine (a) and polished (b) Li anodes after cycling for 10 cycles, respectively. Scale bar: (a) 20 μm ; (b) 20 μm .

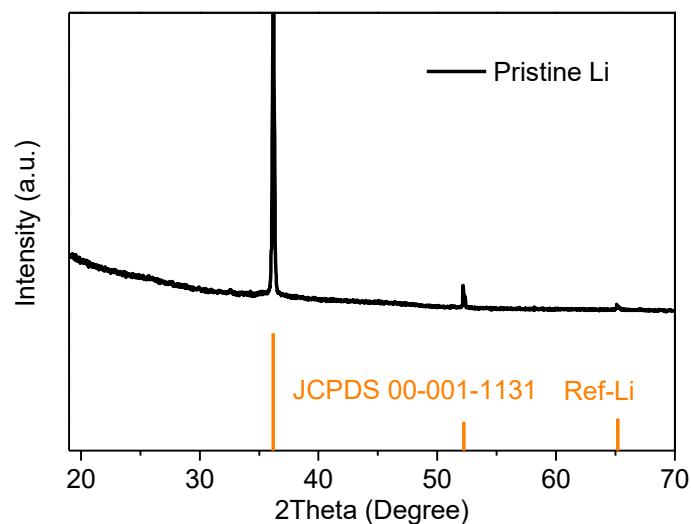


Figure S21. XRD pattern of the pristine Li anode.

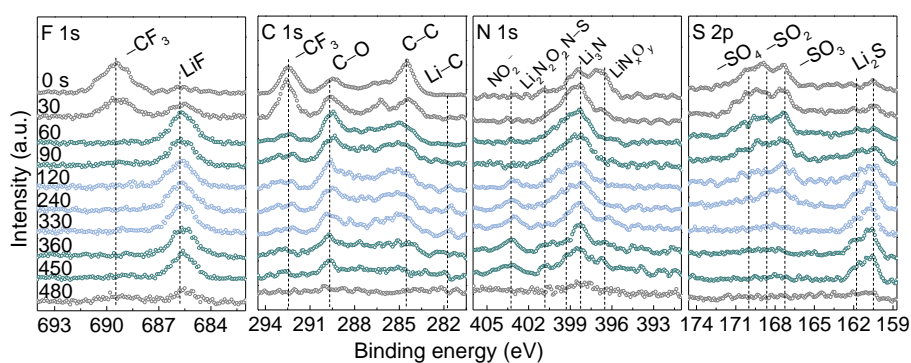


Figure S22. F 1s, C 1s, N 1s, and S 2p XPS depth profiles of the N-SEI film after cycling in an Ar atmosphere.

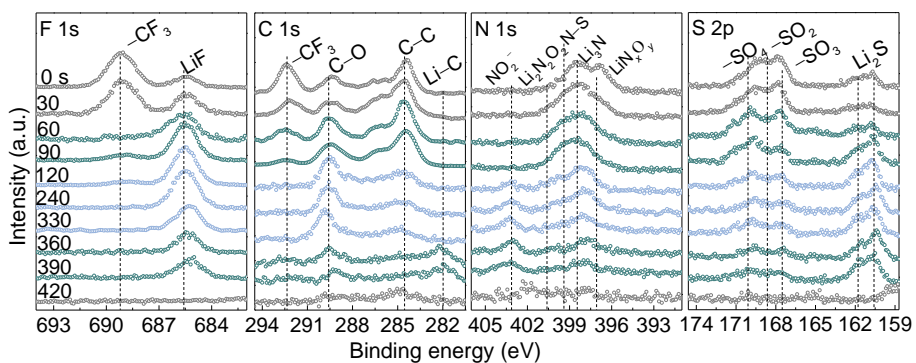


Figure S23. F 1s, C 1s, N 1s, and S 2p XPS depth profiles of the N-SEI film after cycling in an O₂ atmosphere.

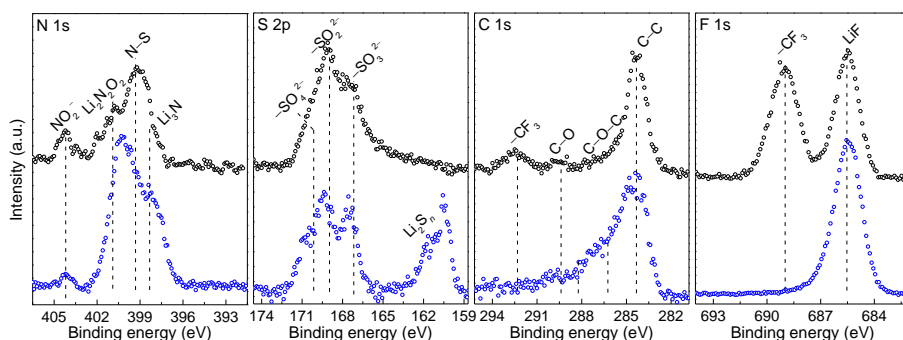


Figure S24. XPS spectra of the SEI formed by chemical aging in LiNO_3 -containing electrolyte before (upper) and after (down) cycling in an Ar atmosphere.

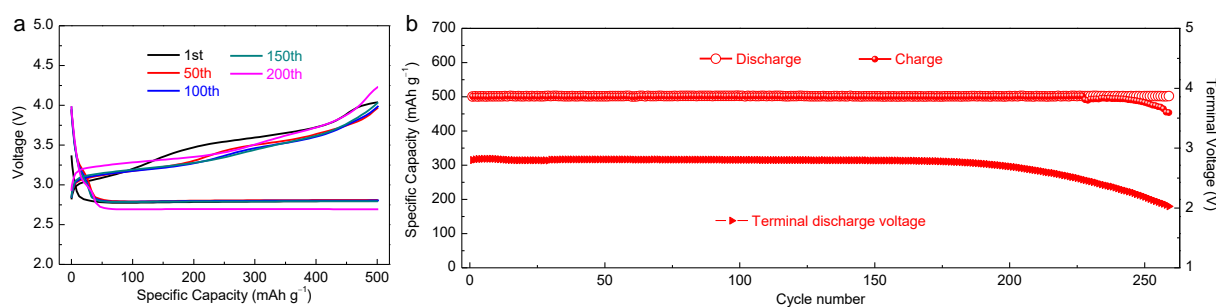


Figure S25. (a) Selected discharge/charge curves of the Ru/rGO-based Li-O_2 batteries with the Li anode polished in a LiNO_3 -free electrolyte under a cutoff capacity of 500 mA h g^{-1} at a current density of 400 mA g^{-1} . (b) Cycling stability and the terminal discharge voltage of the Ru/rGO-based Li-O_2 batteries with the Li anode polished in a LiNO_3 -free electrolyte under a cutoff capacity of 500 mA h g^{-1} at a current density of 400 mA g^{-1} .

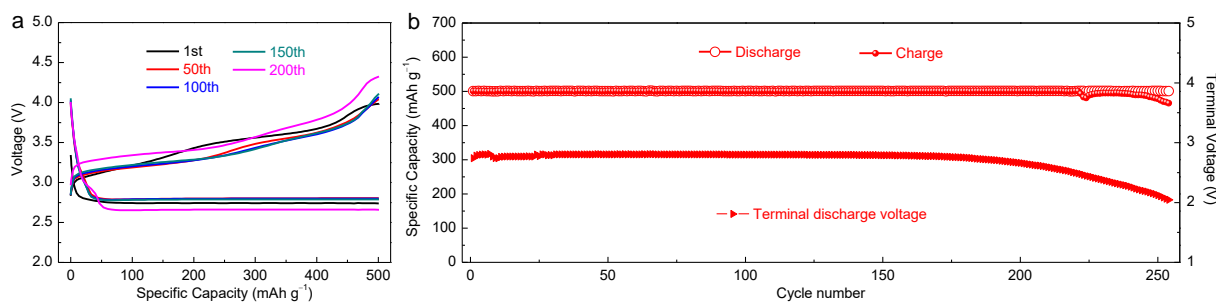


Figure S26. (a) Selected discharge/charge curves of the Ru/rGO-based Li-O_2 batteries with pristine Li anode in $1 \text{ M LiNO}_3/\text{DMSO}$ system under a cutoff capacity of 500 mA h g^{-1} at a current density of 400 mA g^{-1} . (b) Cycling stability and the terminal discharge voltage of the Ru/rGO-based Li-O_2 batteries with pristine Li anode in $1 \text{ M LiNO}_3/\text{DMSO}$ system under a cutoff capacity of 500 mA h g^{-1} at a current density of 400 mA g^{-1} .

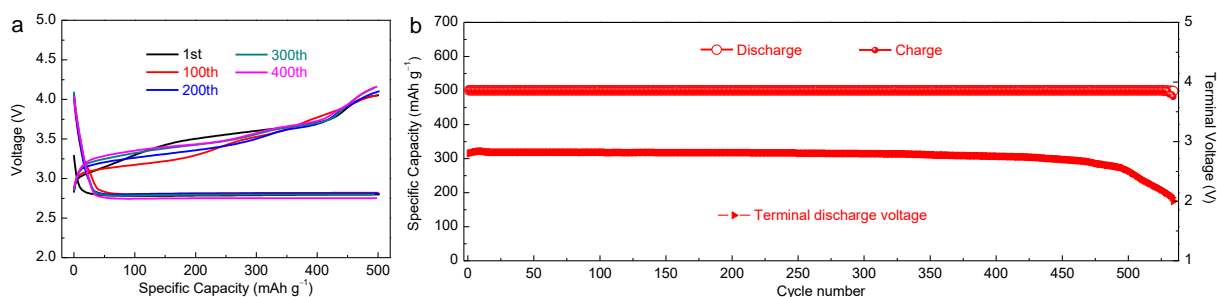


Figure S27. (a) Selected discharge/charge curves of the Ru/rGO-based Li–O₂ battery with polished Li anode in 1 M LiNO₃/DMSO electrolyte system under a cutoff capacity of 500 mA h g⁻¹ at a current density of 400 mA g⁻¹. (b) Cycling stability and the terminal discharge voltage of the Ru/rGO-based Li–O₂ battery with polished Li anode in 1 M LiNO₃/DMSO electrolyte system under a cutoff capacity of 500 mA h g⁻¹ at a current density of 400 mA g⁻¹.

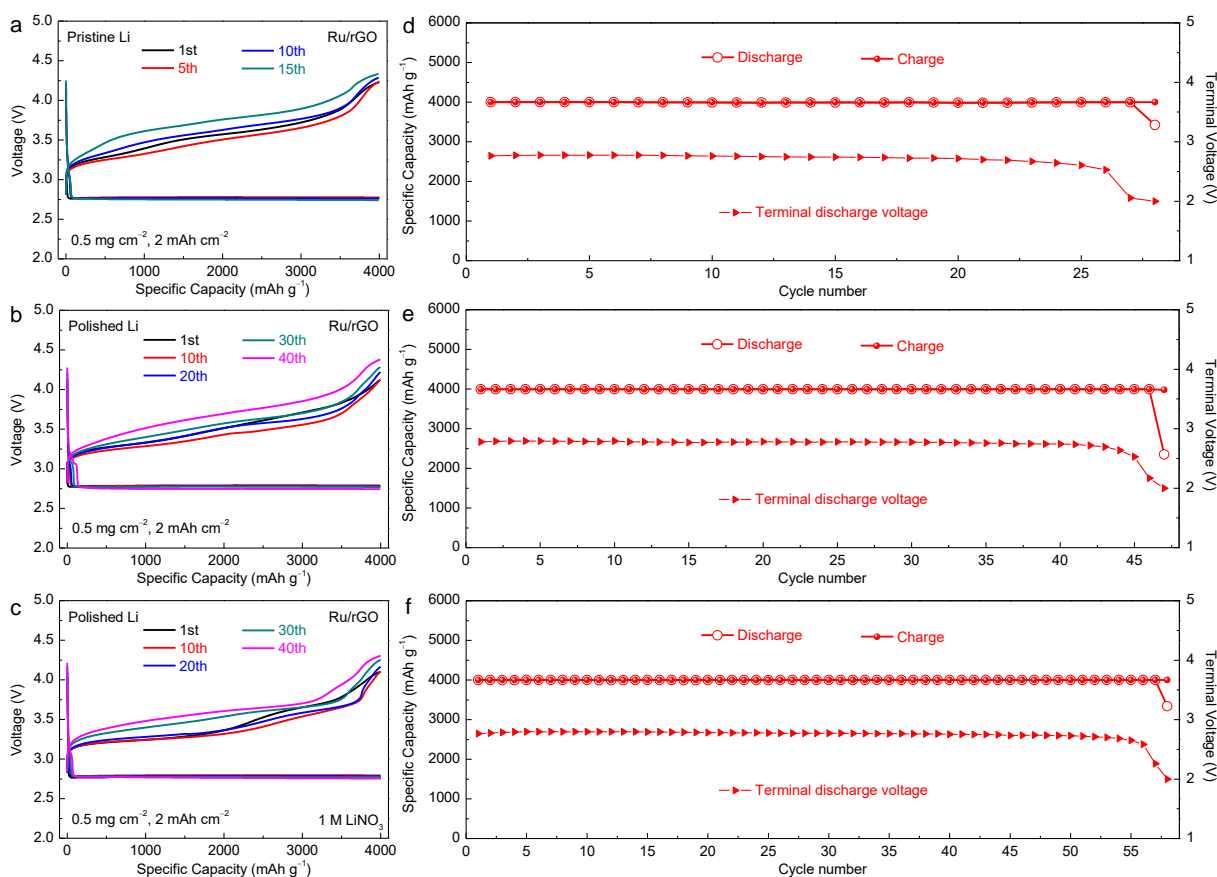


Figure S28. Selected discharge/charge curves of the Ru/rGO-based Li–O₂ batteries with pristine Li anode in 1 M LiClO₄/DMSO electrolyte (a), polished Li anode in 1 M LiClO₄/DMSO electrolyte (b) and 1 M LiNO₃/DMSO electrolyte (c) under a cutoff capacity of 4000 mA h g⁻¹ at a current density of 400 mA g⁻¹, respectively. Cycling stability and the terminal discharge voltage of the Ru/rGO-based Li–O₂ batteries with pristine Li anode in 1 M LiClO₄/DMSO electrolyte (d), polished Li anode in 1 M LiClO₄/DMSO electrolyte (e) and 1 M LiNO₃/DMSO electrolyte (f) under a cutoff capacity of 4000 mA h g⁻¹ at a current density of 400 mA g⁻¹, respectively.

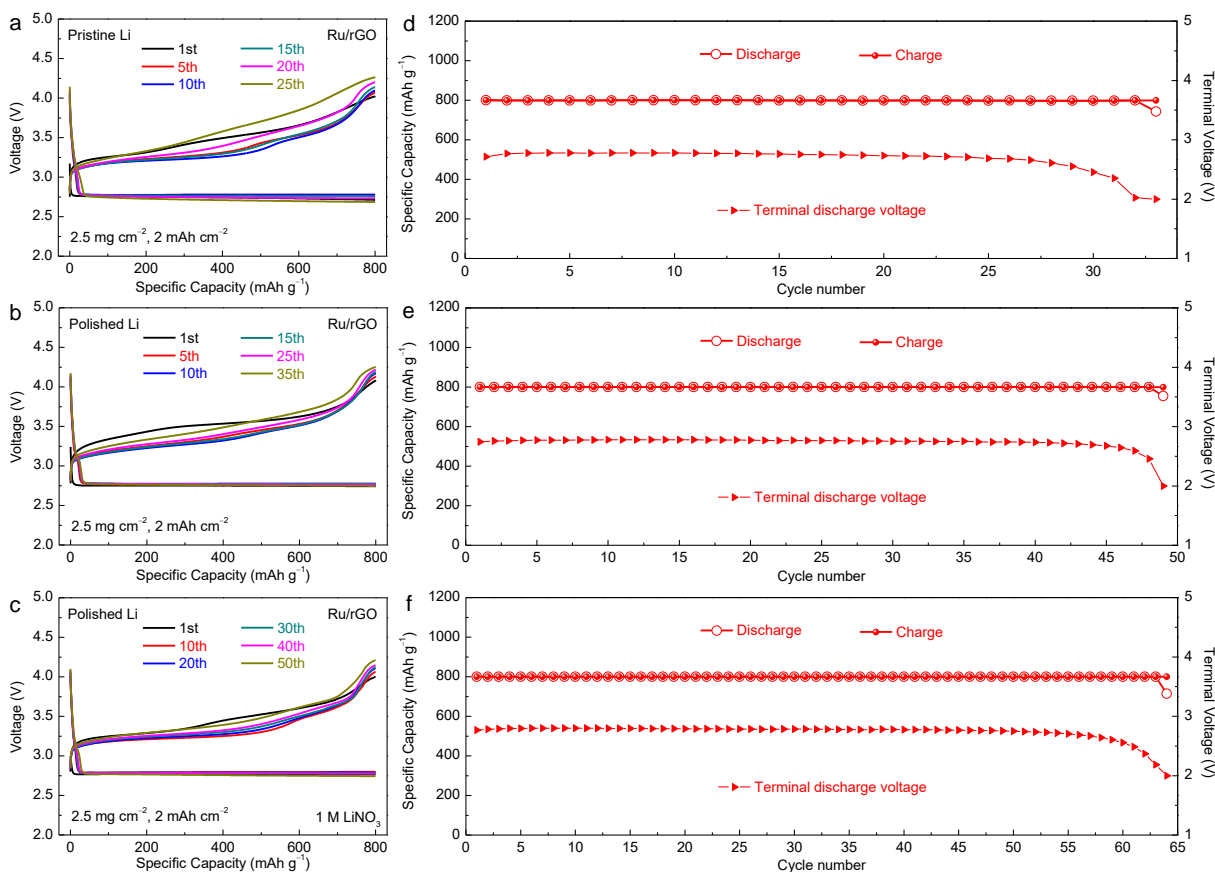


Figure S29. Selected discharge/charge curves of the Ru/rGO-based Li-O₂ batteries with pristine Li anode in 1 M LiClO₄/DMSO electrolyte (a), polished Li anode in 1 M LiClO₄/DMSO electrolyte (b) and 1 M LiNO₃/DMSO electrolyte (c) under a cutoff capacity of 800 mA h g⁻¹ at a current density of 100 mA g⁻¹, respectively. Cycling stability and the terminal discharge voltage of the Ru/rGO-based Li-O₂ batteries with pristine Li anode in 1 M LiClO₄/DMSO electrolyte (d), polished Li anode in 1 M LiClO₄/DMSO electrolyte (e) and 1 M LiNO₃/DMSO electrolyte (f) under a cutoff capacity of 800 mA h g⁻¹ at a current density of 100 mA g⁻¹, respectively.

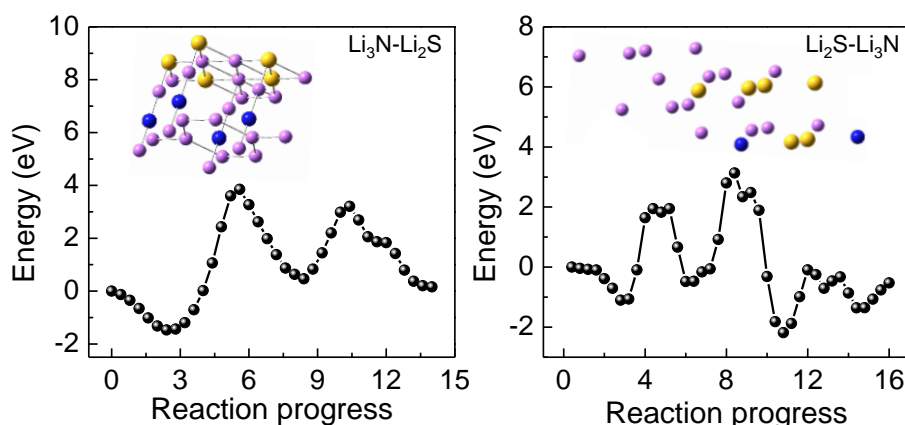


Figure S30. Typical potential energy curves for O₂ molecule migration through the interface between Li₃N and Li₂S. Purple, blue and yellow spheres represent Li, N, S atoms, respectively.

To analyze the possibility of O₂ migration through the interface between two bulk crystal of N-SEI

species. Here, Li_3N and Li_2S , which possess lower energies for preventing O_2 from passing through their crystal channels, were taken as an example for the simulation. Since the crystal system and lattice parameters of the two kinds of crystals are quite different, thus their interface structure is very complicated. In this case, when Li_3N and Li_2S contact with each other, both sides of the composite still retain the main lattice structure of the two crystals, while only the atoms in the interconnection regions could interact. Therefore, we replace some of the atoms in one crystal by the other crystal to create the interface: one keeps the lattice constant of Li_3N (as shown in Figure S30 left), and the other keeps the lattice constant of Li_2S (as shown in Figure S30 right). Then, we calculate the energy of O_2 migration through the interface in these two cases. The results show that the energy barrier of O_2 migration through the interface in both cases is higher than that of O_2 migration through the respective bulk crystal, which could prove that O_2 is more likely to migration through the bulk crystal rather than the interface of two kinds of crystals.

Table S1. Comparison of the electrochemical performance of our LiNO_3 -electropolished Li anode with recent reported Li anodes in an O_2 -saturated symmetric Li cell system.

Strategies	Current density	Capacity	Cycling performance	Overpotential	Ref.
LiNO ₃ -electropolished Li anode	0.5 mA cm ⁻²	1 mA h cm ⁻²	/	0.05 V	This work
	1 mA cm ⁻²	1 mA h cm ⁻²	400 cycles	0.07 V	
	3 mA cm ⁻²	1 mA h cm ⁻²	300 cycles	0.13 V	
SEI-forming additive (boric acid)	0.25 mA cm ⁻²	0.5 mA h cm ⁻²	215 cycles	0.08 V	<i>Adv. Mater.</i> , 2018 , <i>30</i> , 1803270.
DOA-treated Li metal	1 mA cm ⁻²	1 mA h cm ⁻²	~83 cycles	0.025 V	<i>Angew. Chem.</i> , 2018 , <i>130</i> , 12996–13000.
SEI-forming Li salt (LiTFSI)	0.2 mA cm ⁻²	0.5 mA h cm ⁻²	200 cycles	0.05 V	<i>Adv. Mater.</i> , 2018 , <i>30</i> , 1704841.
Phosphorene-coated Li metal	0.1 mA cm ⁻²	0.05 mA h cm ⁻²	500 cycles	~0.03 V	ACS Nano, 2018 , <i>12</i> , 4419–4430.
	0.2 mA cm ⁻²	0.1 mA h cm ⁻²	/	~0.05 V	
	0.5 mA cm ⁻²	0.25 mA h cm ⁻²	100 cycles	~0.07 V	
	1 mA cm ⁻²	0.5 mA h cm ⁻²	/	~0.1 V	
	2 mA cm ⁻²	1 mA h cm ⁻²	100 cycles	~0.13 V	
3 mA cm ⁻²	1.5 mA h cm ⁻²	/	~0.15 V		
Electrolyte regulation (10 wt.% SiO ₂ /1 M LiCF ₃ SO ₃ /TEGDME)	0.1 mA cm ⁻²	0.1 mA h cm ⁻²	350 cycles	0.03 V	<i>Matter</i> , 2019 , <i>1</i> , 881–892.

Table S2. EIS fitting results obtained using the electric equivalent circuit of Figure S6.

Cycle number	Pristine Li		LiNO ₃ -polished Li	
	R _s (Ω)	R _{int} (Ω)	R _s (Ω)	R _{int} (Ω)
5	3.08	85.31	2.22	47.39
20	9.79	38.46	2.21	46.49
50	25.69	–	2.35	49.14

Table S3. Comparison of the electrochemical performance of our LiNO₃-electropolished Li anode with recent reported Li anodes in a Li–O₂ battery system.

Strategies	Cathode	Current density	Capacity	Cycling performance	Ref.
LiNO ₃ -electropolished Li anode	Ru/rGO	400 mA g ⁻¹	500 mA h g ⁻¹	415 cycles	This work
	rGO	400 mA g ⁻¹	500 mA h g ⁻¹	375 cycles	
SEI-forming additive (boric acid)	CNT sponge	300 mA g ⁻¹	1000 mA h g ⁻¹	146 cycles	<i>Adv. Mater.</i> , 2018 , <i>30</i> , 1803270.
DOA-treated Li metal	Ketjen black	100 mA g ⁻¹	500 mA h g ⁻¹	65 cycles	<i>Angew. Chem.</i> , 2018 , <i>130</i> , 12996–13000.
FEC-treated Li metal	Super P (SP)	300 mA g ⁻¹	1000 mA h g ⁻¹	106 cycles	<i>Adv. Mater.</i> , 2015 , <i>27</i> , 5241–5247.
SEI-forming Li salt (LiTNFSI)	Ketjen black	72 mA g ⁻¹	500 mA h g ⁻¹	50 cycles	<i>Adv. Mater.</i> , 2018 , <i>30</i> , 1704841.
Phosphorene-coated Li metal	Ketjen black	250 mA g ⁻¹	1000 mA h g ⁻¹	50 cycles	<i>ACS Nano</i> , 2018 , <i>12</i> , 4419–4430.
Concentrated LiTFSI-3DMSO	CNT	~140 mA g ⁻¹	600 mA h g ⁻¹	90 cycles	<i>Adv. Energy Mater.</i> , 2017 , <i>7</i> , 1602605.
LiNO ₃ /DMA-soaked Li metal	Csp carbon	~22 mA g ⁻¹	~220 mA h g ⁻¹	80 cycles	<i>J. Am. Chem. Soc.</i> , 2013 , <i>135</i> , 2076–2079.
Electrochemical precharging Li metal	CNT	200 mA g ⁻¹	500 mA h g ⁻¹	180 cycles	<i>Adv. Energy Mater.</i> , 2018 , <i>8</i> , 1702340.
TBF-modified Li anode	Ru/CNT	300 mA g ⁻¹	1000 mA h g ⁻¹	106 cycles	<i>Adv. Mater.</i> 2017 , <i>29</i> , 1606552.
Al ₂ O ₃ /PVdF-HFP protective layer	Co ₃ O ₄ /SP	200 mA g _{sp} ⁻¹	1000 mA h g _{sp} ⁻¹	80 cycles	<i>Electrochem. Commun.</i> , 2014 , <i>40</i> , 45–48.
Electrolyte regulation (10 wt.% SiO ₂ /1 M LiCF ₃ SO ₃ /TEGDME)	Ru/CNT	300 mA g ⁻¹	1000 mA h g ⁻¹	168 cycles	<i>Matter</i> , 2019 , <i>1</i> , 881–892.